Talanta 89 (2012) 223–230

Contents lists available at SciVerse ScienceDirect

Talanta

journal homepage: www.elsevier.com/locate/talanta

Influence of grain topography on near infrared hyperspectral images

Marena Manley[a,*], Cushla M. McGoverin[a], Paulina Engelbrecht[a], Paul Geladi[a,b]

[a] Department of Food Science, Stellenbosch University, Private Bag X1, Matieland (Stellenbosch), 7602, South Africa
[b] Unit of Biomass Technology and Chemistry, Swedish University of Agricultural Sciences, KBC Huset, Linnaeus vaeg 6, SE 901 87 Umeå, Sweden

ARTICLE INFO

Article history:
Received 29 June 2011
Received in revised form 19 October 2011
Accepted 27 November 2011
Available online 9 December 2011

Keywords:
Barley
Classification gradients
Principal component analysis
Sorghum
Topography
Wheat

ABSTRACT

Near infrared hyperspectral imaging (NIR-HSI) allows spatially resolved spectral information to be collected without sample destruction. Although NIR-HSI is suitable for a broad range of samples, sizes and shapes, topography of a sample affects the quality of near infrared (NIR) measurements. Single whole kernels of three cereals (barley, wheat and sorghum), with varying topographic complexity, were examined using NIR-HSI. The influence of topography (sample shape and texture) on spectral variation was examined using principal component analysis (PCA) and classification gradients. The greatest source of variation for all three grain types, despite spectral preprocessing with standard normal variate (SNV) transformation, was kernel curvature. Only 1.29% (PC5), 0.59% (PC6) and 1.36% (PC5) of the spectral variation within the respective barley, wheat and sorghum image datasets was explained within the principal component (PC) associated with the chemical change of interest (loss of kernel viability). The prior PCs explained an accumulated total of 91.18%, 89.43% and 84.39% of spectral variance, and all were influenced by kernel topography. Variation in sample shape and texture relative to the chemical change of interest is an important consideration prior to the analysis of NIR-HSI data for non-flat objects.

1. Introduction

Near infrared (NIR) spectroscopy has been used throughout the food industry for decades [1]. The recent adaptation of NIR spectroscopy for imaging purposes (near infrared hyperspectral imaging (NIR-HSI) or near infrared chemical mapping) allows spatially resolved spectral information to be collected [2]. NIR-HSI retains the advantages of NIR spectroscopy, namely no sample preparation or destruction, and the ability to examine several constituents simultaneously. In addition, NIR-HSI is able to identify and locate chemically or physically similar regions within a sample. As a combination of imaging and NIR spectroscopy, NIR-HSI is subject to error arising from both techniques [3–5]. Consequently, topography (sample shape and texture) of the sample affects the collected NIR spectra [2,6]. The influence of topography on hyperspectral imaging data was previously shown in a study of bruised mushrooms [5]. Path length differences and non-uniform lighting, caused by sample curvature, resulted in higher reflectance intensities recorded from sampling points closest to the detector. The influence of topography was subsequently minimised by applying preprocessing methods to spectral datasets [6]. Mushroom topographic effects were explained by the first principal component (PC1) of a principal component analysis (PCA) applied to raw data [5]. The application of mean normalisation to the spectral dataset effectively removed the influence of mushroom curvature [5]. Many agricultural samples have more complex topographies than mushrooms and shape/surface roughness effects may not be so easily diminished or described. It was shown that despite preprocessing (multiplicative scatter correction or standard normal variate combined with Savitzky-Golay smoothing), sample curvature dominated PC1 of a wheat image dataset when diffusion of conditioning water was investigated [7].

When using a pushbroom imaging system (line scanner), an attempt is made to create a rectangle of illumination that is homogeneous along its length. The intensity across the width of the illumination rectangle may vary because the camera only detects the central region. This works well with flat or semi-flat surfaces; with round objects a number of irregularities are created: (1) the maximum intensity and size of the rectangle of illumination is dependent on the height above the background on which the samples are placed; (2) there will be shades on the vertical sides of the objects; and (3) the reflection geometry will be different across the objects because of curvature. These effects are repeated on a miniature scale if there is a surface roughness, hairiness or porosity.

The detection of kernel viability was assessed in an earlier study [8]. In this study it was observed that chemical variation relating to viability was only explained in the lowest variance PCs; barley and sorghum viability was explained in PC5 and wheat viability in PC6.

* Corresponding author. Tel.: +27 21 808 3511; fax: +27 21 808 3510.
E-mail addresses: mman@sun.ac.za (M. Manley), cushla.mcgoverin@gmail.com (C.M. McGoverin), paulina.engelbrecht@gmail.com (P. Engelbrecht), paul.geladi@slu.se (P. Geladi).

0039-9140/$ – see front matter © 2011 Elsevier B.V. All rights reserved.
doi:10.1016/j.talanta.2011.11.086

The sources of spectral variation explained in the higher variance PCs were investigated in this study. PC1 calculated from conventional NIR spectra normally explains physical variation, e.g. due to particle size differences. It is thus likely that these higher variance PCs also explain variation due to physical differences. In the case of NIR imaging these differences are probably due to variation in sample height, shape or surface texture. An investigation into the effect of grain topography on the observation of a more subtle (in terms of NIR) chemical process, i.e. grain viability, is presented; specifically, the effect of barley, wheat and sorghum topography on PCA applied to image datasets recorded from grains exposed to 0–24 h of incubation (germination).

2. Materials and methods

2.1. Samples and sample preparation

This study was carried out in conjunction with a study which examined the efficacy of NIR-HSI for the identification of non-viable barley, wheat and sorghum kernels [8,9]. The wheat (cultivar – Duzi), barley (cultivar – Puma) and sorghum (cultivar – South African landrace 4442) samples were kindly provided by the Agricultural Research Council – Small Grain Institute (Stellenbosch, South Africa), SAB Maltings (Pty) Ltd (Caledon, South Africa) and PANNAR (Pty) Ltd (Greytown, South Africa) respectively. From each cereal, six subsets of 25 kernels were randomly selected. Five subsets from each of the barley, wheat and sorghum samples were individually placed in petri-dishes lined with 2 layers of Whatman no.1 filter paper (Kimix Chemical and Laboratory Supplies, Cape Town, South Africa), and 3 mL of distilled water was added. A single subset from each of the cultivars was incubated (to initiate germination) at 19 °C for each of the following time periods: 6, 9, 12, 18 and 24 h. One subset from each cultivar was not treated with water or incubated and kept as a control (0 h). All samples were subsequently frozen at −80 °C for 24 h and freeze dried (Virtis, Benchtop 6.6, The Virtis Company, Gardiner, USA) for 72 h. All freeze dried samples were vacuum sealed and stored at ambient temperature for not more than three weeks until NIR-HSI data was collected. After collection of imaging data each kernel was analysed for viability, i.e. whether germination has commenced (non-viable kernel) or not (viable kernel) [8]. Kernel viability was assessed using the tetrazolium test. Barley kernels were cut longitudinally and soaked in a 1% (w/v) 2,3,5-triphenyl-tetrazolium chloride (Merck (Pty) Ltd, Germiston, South Africa) solution at 40 °C for 30 min; the same procedure was followed for wheat and sorghum kernels, however, a 0.5% (w/v) 2,3,5-triphenyl-tetrazolium chloride solution and 60 min was used. In fully viable kernels the embryo, scutellum and aleurone layer were stained bright pink-red but remained unstained in non-viable kernels.

2.2. Near infrared hyperspectral imaging

2.2.1. Data collection

Near infrared hyperspectral images were acquired using a SisuCHEMA short wave infrared (SWIR) hyperspectral imaging system (Specim, Spectral Imaging Ltd, Oulu, Finland), consisting of a prism–grating–prism spectrograph coupled with a 2-D array HgCdTe detector. The SisuCHEMA system comprises a pushbroom (line scan) imaging configuration controlled by the ChemaDAQ software. An integration time of 2.7 ms per line was used. A lens with a 50 mm wide field-of-view was used and a maximum length of 100 mm was imaged. Each spectrum (i.e. pixel) collected represented a 150 μm × 150 μm area. Spectra were acquired from 1000 to 2498 nm with 6.3 nm intervals, resulting in images with the maximum dimensions of 320 (x) × 583 (y) × 239 (λ). Internal dark and external white reference standards were used for image calibration. The raw image was corrected automatically in Evince version 2.4.0 (Umbio AB, Umeå, Sweden). The images were corrected and transformed to pseudo-absorbance from instrument measurement counts (A/D converter counts) by subtracting the dark reference image from the raw images and dividing this sum by the total reflectance spectrum of the dark reference image subtracted from a white reference image:

$$I_{\lambda,n} = -\log\left[\left(\frac{S_{\lambda,n} - B_{\lambda,n}}{W_{\lambda,n} - B_{\lambda,n}}\right) \times 0.50\right]$$

where n = pixel index variable ($n = 1, \ldots, N$); $I_{\lambda,n}$ = standardised absorbance intensity at pixel n at wavelength λ; $S_{\lambda,n}$ = sample image intensity at pixel n at wavelength λ; $B_{\lambda,n}$ = dark reference image intensity at pixel n at wavelength λ; $W_{\lambda,n}$ = dark reference image intensity at pixel n at wavelength λ; 0.50 = total reflectance of the standard used.

The hyperspectral imaging data for each cereal was collected in a single image. From each subset 10 kernels (12 in the case of sorghum) were randomly selected to be imaged. These 60 kernels (72 in the case of sorghum) were arranged into 12 rows and five (or six) columns; the kernels from each subset were grouped together over two rows, however, the order of the subset rows was randomised with respect to incubation time. Kernels were positioned germ up on the silicon carbide sandpaper lined sample stage. The dorsal or rounded sides were thus imaged with the ventral or creased side on the sandpaper. The kernels were positioned such that the germ of all the grains pointed in the same direction; in this case to the right (to the left on the NIR images).

2.2.2. Data analysis

Evince version 2.4.0 was used for all data processing and analysis of hyperspectral image data. The images of each grain were divided into smaller images representing subsets based on incubation time. These were subsequently arranged using the mosaic technique in chronological order for ease of interpretation, before data analysis commenced. The image of each grain type was analysed individually, e.g. all 60 kernels of the barley image were analysed together. Principal component analysis was applied to mean-centered data to identify and classify unwanted pixels, e.g. outliers, silicon carbide background, dead pixels, shading errors and edge effects, as outlined in Williams et al. [10]. The unwanted pixels were removed from the dataset. Standard normal variate (SNV) transformation followed by mean-centering was applied to the remaining data and PCA was applied to the SNV transformed data [8]. Alternatively, multiplicative scatter correction (MSC), first derivative (1D) and second derivative (2D) preprocessing were also evaluated. Exploratory analysis of the score plots and images utilised the interactive feature of Evince, i.e. when a region was selected in the score plot the same pixels were highlighted in the score image and vice versa; this is often referred to as brushing [11].

To identify the underlying source of variation explained in each PC, classification gradients were used. Classification gradients were defined individually for each PC. To define the classification gradients the scores range for a specific PC was divided into between four and six successive groups. Hence, the first group consisted of pixels with the most negative score values for the specific PC and the last group consisted of pixels with the most positive score values. Each of these groups was assigned a distinct colour in the score plot which was subsequently projected onto the score image to create a classification image. These classification images allowed the influence of grain topography on PCA results to be identified.

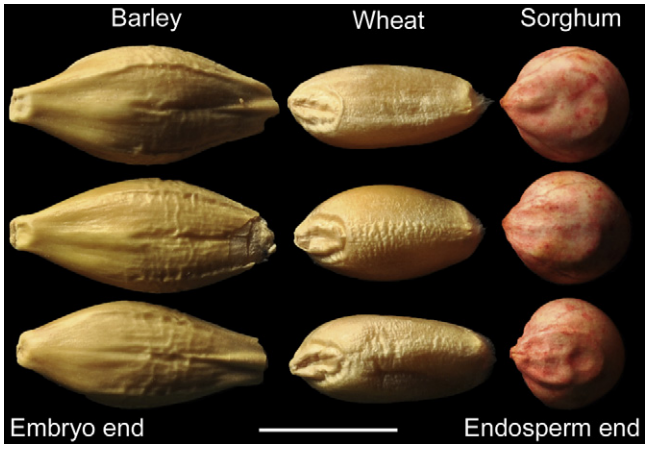

Fig. 1. Barley (left), wheat (centre) and sorghum (right) grains have significantly different topographies. The grains are positioned with the germ showing upwards and to the left of the digital image. Scale bar is 5 mm. This digital image was taken using a Nikon D90 with a Sigma 70 mm F2.8 EX DG macro lens.

3. Results and discussion

Kernel topography and surface roughness influence a NIR reflectance image by altering reflection and scattering. Classification gradients were defined in score plots and projected onto the respective score images to allow visual assessment of topographical effects contributing to the spectral variation explained within each PC. Only the results obtained using SNV preprocessing are presented; substitution of SNV with MSC, 1D or 2D preprocessing lead to similar conclusions. Barley, wheat and sorghum kernels have significantly different topographies (Fig. 1). Sorghum is a smooth surfaced nearly spherical grain; wheat is a fairly cylindrical grain with a textured surface and prominent indentation around the embryo; and barley, the largest of the three grains is ovoid with an intermediately textured hull.

3.1. Barley

Within the dataset of the barley kernel image, a distinct difference between viable and non-viable kernels was not clearly observed until PC5 (Fig. 2) [8]. The greatest source of spectral variation, explained in PC1, was attributed to kernel curvature. This could clearly be seen when classification gradients were made in the direction of PC1 from negative to positive scores. Negative PC1 scores (red and dark blue in Fig. 2) were associated with the higher rounded or dorsal part of the barley kernels which would have been closest to the light source and detector. Positive PC1 scores (green and orange) were associated with the lower awn (germ side) and basal ends which would have been furthest from the light source and detector. The absence of strong peaks in the loading line plot of PC1 (Fig. 3) indicated this PC1 was primarily describing scattering effects due to kernel shape and the textured hull rather than chemical composition. This is further emphasised by an examination of the SNV preprocessed average spectra of the groups defined along PC1 (Fig. 4). A baseline shift was observed from the most negative to the most positive group along PC1; a baseline shift is generally associated with scattering effects.

The negative and positive score extremes of PC2 (red and green respectively in Fig. 2) were largely associated with the kernel edges. This could have been due to some remaining shading effects not removed during sample cleaning. PC2 scores around zero were associated with the higher dorsal part of the kernel with distinction noticeable between the starchy endosperm having positive scores (light blue) and the embryo with negative scores (dark blue). The loading line plot of PC2 contained a series of prominent peaks attributed to starch, protein and water (Fig. 3) [12]. PC2 explains the variation due to proximate grain composition, thus the presence of and variation in starchy endosperm, protein and moisture.

In PC3 the most negative score values (red in Fig. 2) were associated with kernel edges. As in PC2 the less extreme negative PC3 scores (dark blue) were associated with the embryo region of the dorsal part of the kernel and the less extreme positive PC3 scores (light blue) with the starchy endosperm. The most positive scores

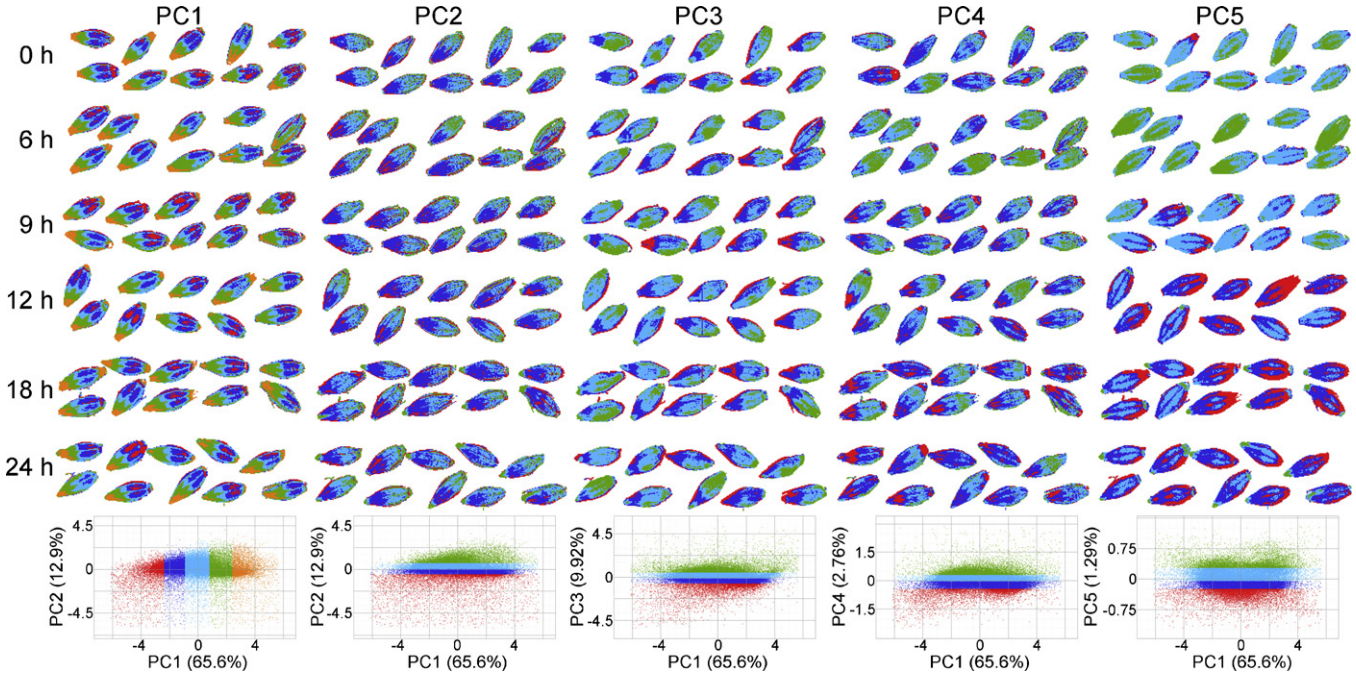

Fig. 2. Barley classification gradient images and PC score plots of the first five principal components (PCs). By defining a classification gradient within the score plots, the contribution of kernel topography to the PC could be assessed. The colours shown in the score plots correspond to the colours in the classification gradient image directly above. (For interpretation of the references to colour in this figure legend, the reader is referred to the web version of the article.)

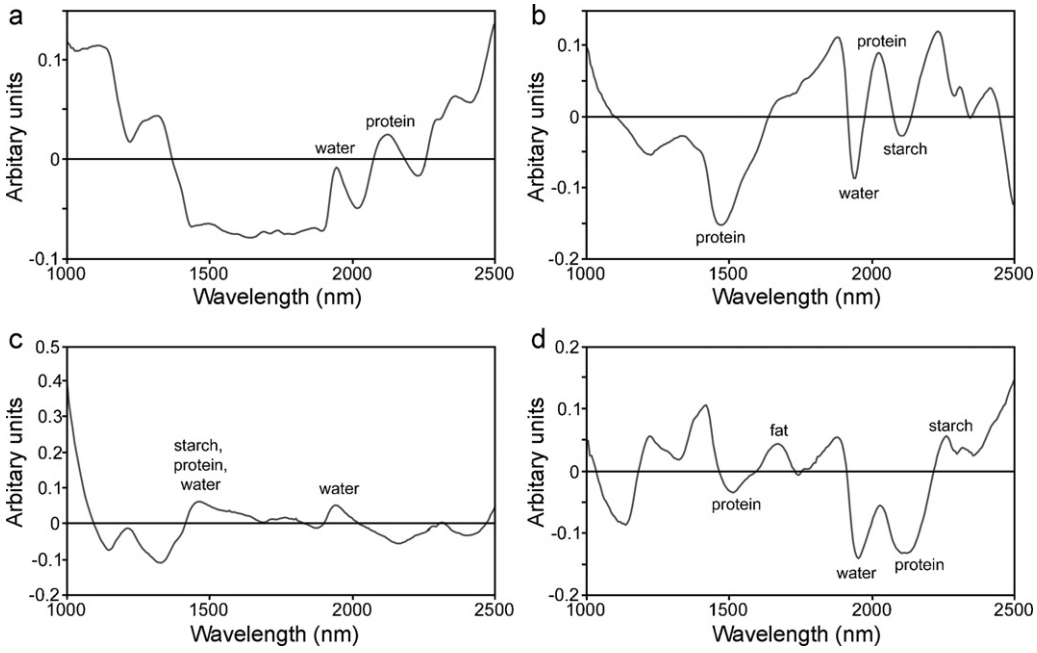

Fig. 3. Principal component analysis loading line plots of the barley image dataset. (a) The absence of prominent peaks in the loading line plots of principal component one (PC1) indicated this PC was primarily due to scattering effects. (b) Strong peaks in PC2 loadings were indicative of chemical differences involving starch, protein and water. (c) The loadings of PC3 were attributed to scattering and physical effects. (d) The strong peaks of PC4 were indicative of the differences between viable and non-viable kernels.

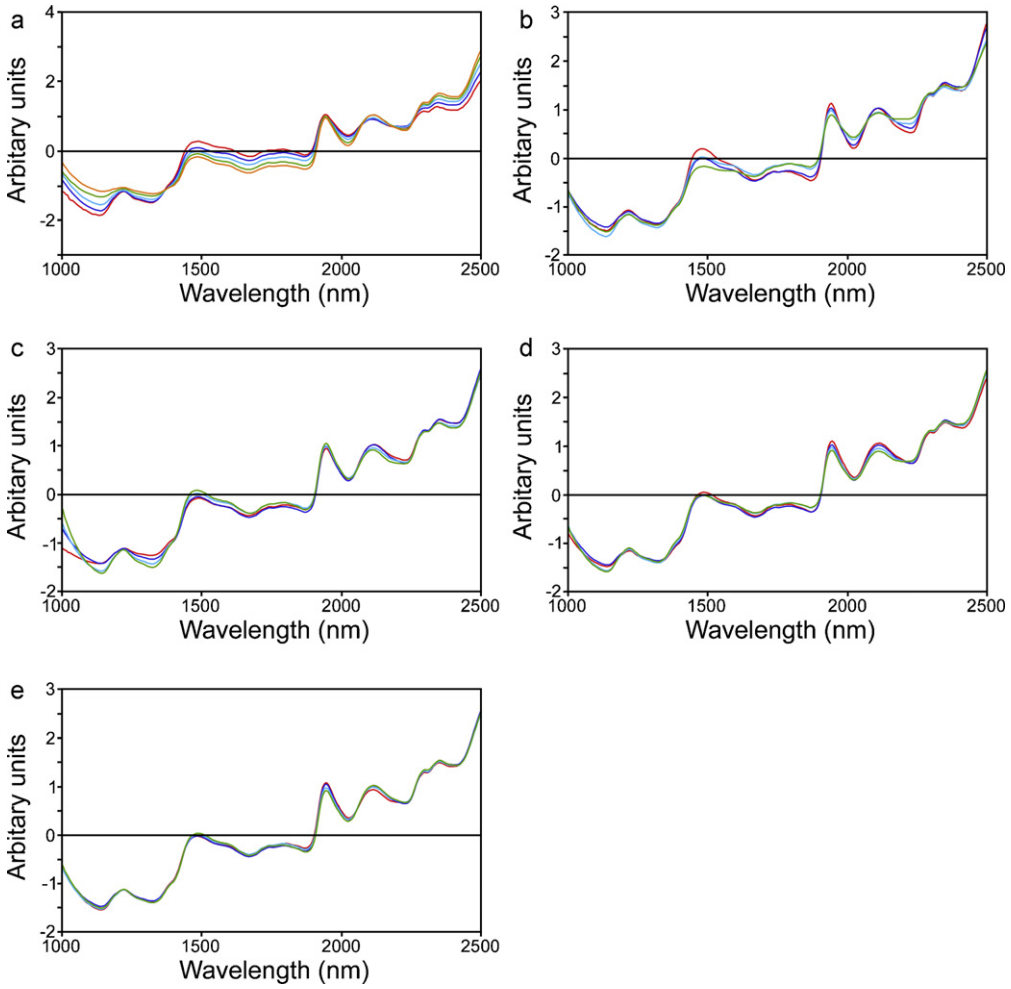

Fig. 4. The SNV preprocessed average spectra for the groups defined using PC1 (a), PC2 (b), PC3 (c), PC4 (d) and PC5 (e). The spectrum colour corresponds to the group colour in Fig. 2. (For interpretation of the references to colour in this figure legend, the reader is referred to the web version of the article.)

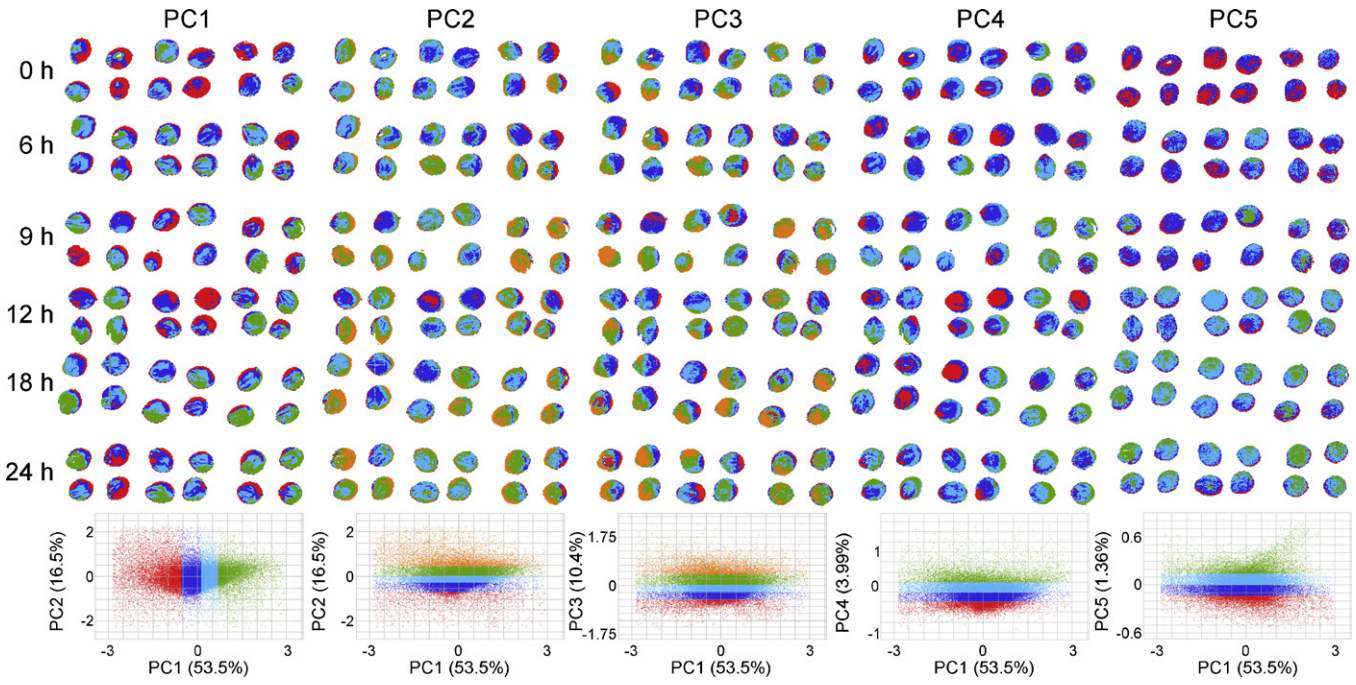

Fig. 5. Classification gradient images of sorghum kernels for PC1–PC5. The selection of the classification gradients in the direction of each PC are shown in the PC score plots. The colours shown in the score plots correspond to the colours in the classification gradient image directly above. (For interpretation of the references to colour in this figure legend, the reader is referred to the web version of the article.)

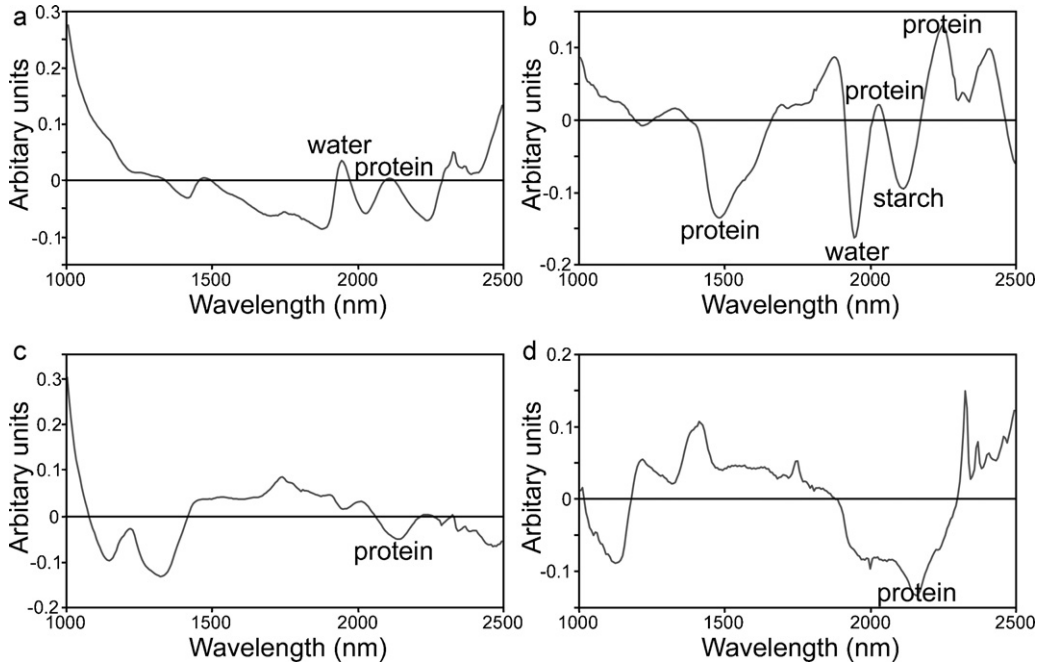

Fig. 6. Principal component analysis loading line plots of the sorghum image dataset. (a) The absence of prominent peaks in the loading line plots of principal component one (PC1) indicated this PC was primarily due to scattering effects. (b) Strong peaks in PC2 loadings were indicative of chemical differences involving starch, protein and water. (c) The loadings of PC3 were attributed to scattering and physical effects. (d) PC4 characterised both physical and chemical effects; the strong peaks of PC4 were indicative of the differences between viable and non-viable kernels.

of PC3 (green) were largely associated with the lower basal end of the kernel. The topographic influence within PC3 was apparent in the loading line plot which contained no prominent peaks (Fig. 3).

In PC4 the first evidence of a difference between viable and non-viable kernels was observed (Fig. 2); however, the lowest regions (awn that is close to the germ and furthest away from the light source and detector) of the kernel were still associated with the most negative scores (red). The subsequent classification gradients referred to the embryo (dark blue) and starchy endosperm (light blue and green) regions of the kernel. The light blue and green coloured regions in the score image begin to indicate the difference between viable and non-viable kernels. The starchy endosperm of the non-viable kernels is indicated as light blue and that of the viable kernels as green. This chemical variation explained in PC4 was also apparent in the loading line plot as peaks associated with starch, fat and protein were heavily weighted (Fig. 3) [12]. In PC5 the

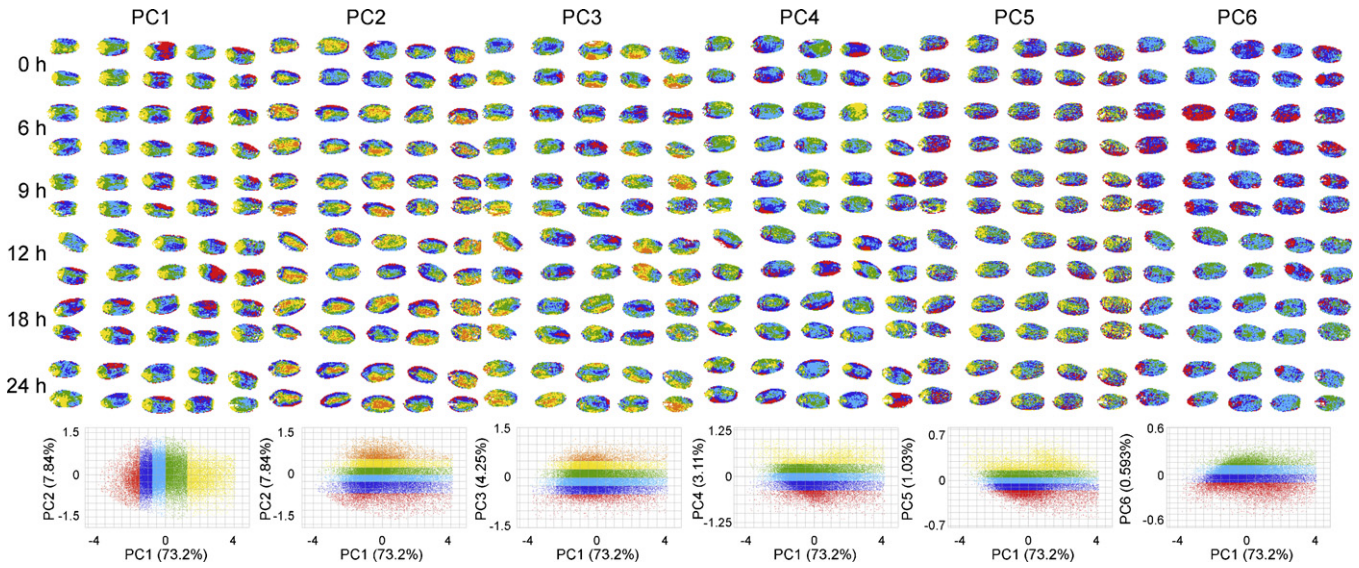

Fig. 7. Classification gradient images of wheat kernels for PC1–PC6. The selection of the classification gradients in the direction of each PC are shown in the PC score plots. The colours shown in the score plots correspond to the colours in the classification gradient image directly above. (For interpretation of the references to colour in this figure legend, the reader is referred to the web version of the article.)

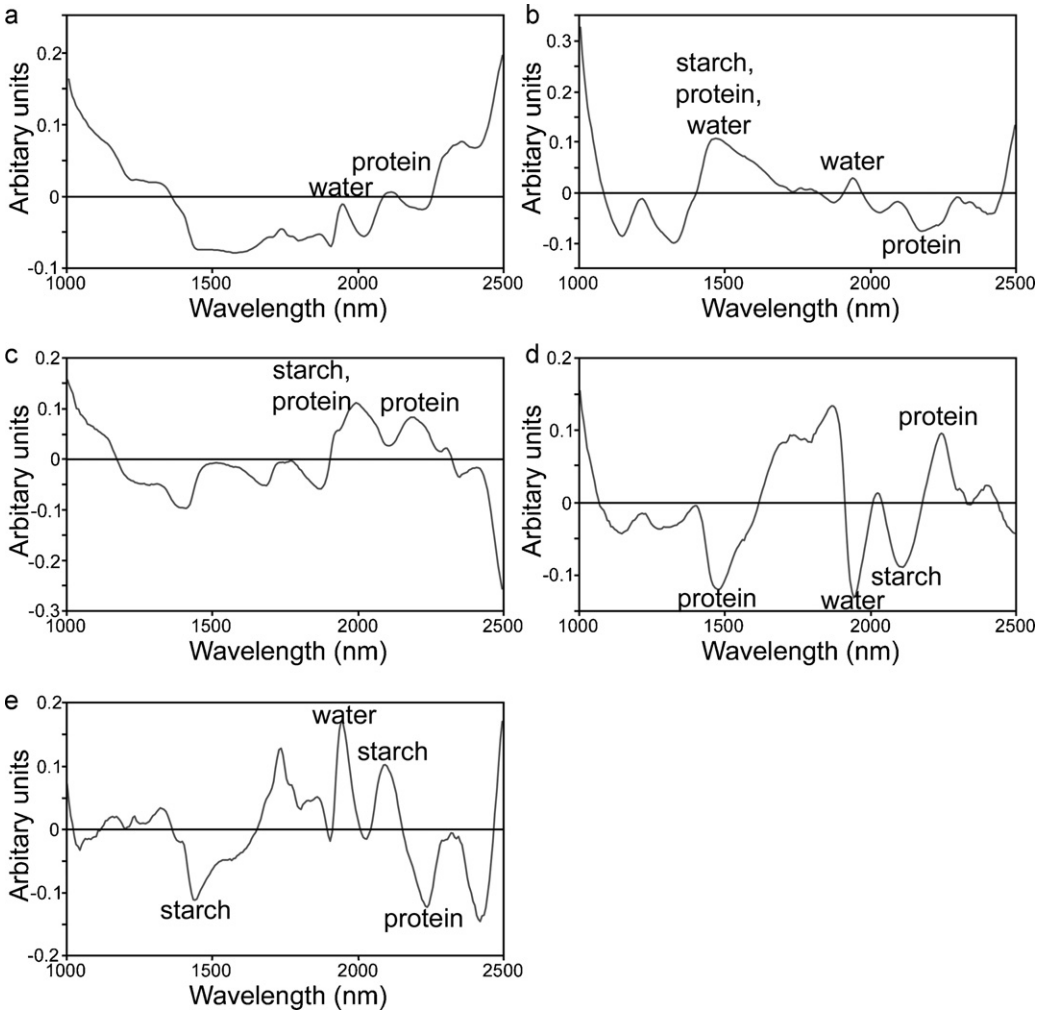

Fig. 8. Principal component analysis loading line plots of the wheat image dataset. (a) The absence of prominent peaks in the loading line plots of principal component one (PC1) indicated this PC was primarily due to scattering effects. (b) Strong peaks in PC2 loadings were indicative of chemical differences involving starch, protein and water. PC3 (c), PC3 (d) PC4 and (e) PC5 contained both physical and chemical effects, the ratio of which decreased from PC3 to PC5.

distinction between viable and non-viable kernels was clear with green indicating viable kernels. The indication of viability is probably possible due to release of enzymes and break down of starches. The differentiation of viability observed in PC5 is explained in more detail in McGoverin et al. [8].

Examination of the average SNV corrected spectra for each of the groups defined along PC1–PC5 (Fig. 4) clearly indicated a reduction in baseline differences between the groups from PC1 to PC5. Baseline differences are associated with physical effects. When PC1 was used to define the classification gradient, the groups were primarily separated on the basis of topography, hence the average spectra of each PC1 group exhibited the largest baseline differences. Each successive PC exhibited less baseline differences. In conventional NIR spectroscopy PC1 usually accounted for most of the physical differences while in NIR imaging more PCs are required. The baseline differences between the respective groups decreased from PC1 to PC5 because chemical changes accounted for a greater proportion of the variance explained by the lower variance PCs. Chemical differences were apparent in the different peak intensities within the average spectra.

The variation explained by PC1 after PCA was applied to the image data of barley kernels was primarily topographical. The variation explained by this PC could be attributed to physical and thus scattering effects due to shape and surface roughness. The loading line plot and score image of PC3 also indicated that the variation explained by this PC was primarily due to scattering effects. The variation explained by PC2 was due to proximate compositional differences within and between the kernels, while the variation explained by PC4 was, to some extent, due to the changes caused by germination of the kernels.

3.2. Sorghum

The sorghum kernels were smaller than those of both barley and wheat, and the variability in the height of the rounded or dorsal side of the kernel was greater for sorghum than wheat and barley. This height variability was observed within PC1 (Fig. 5). PC1 of the sorghum dataset was based on curvature; negative PC1 score values (red and dark blue in Fig. 5) were associated with the kernel edges and positive PC1 score values (light blue and green) with the more flat or dorsal part of the kernel. The effect of the kernel edges not being consistent could be due to some shading effects still being present. The extremes of PC2 (red and orange) were assigned to the edges (possible shading) of sorghum grain and the moderate PC2 score values (light blue and green) to the higher dorsal parts of sorghum. In PC3 positive score values (green and orange) were assigned to the embryo end and negative score values (red and dark blue) to the starchy endosperm, referring to the proximate composition of the grain. The loading line plots of PC1–PC3 of sorghum were similar to those of the barley image dataset. The score image of PC4 was the first indication a viable/non-viable kernel distinction could be derived from the NIR-HSI data, however, this distinction was clearer in PC5 where negative scores (red and dark blue) were assigned to viable kernels and positive scores (light blue and green) to non-viable kernels. The breakdown of starch due to the onset of germination was most likely the cause for this clear distinction between the viable and non-viable kernels. PC4 was complicated by an association of negative scores (red and dark blue) with the embryo of the sorghum kernels still being prominent. In concordance with the barley image dataset the baseline differences between the average SNV corrected spectra of each of the defined groups decreases with increasing PC (decreasing explained variance); again indicating a decrease in the contribution of physical variance with increasing PC.

As in the barley image dataset the first PC accounted for curvature observed by differences in scattering (Fig. 6). However, unlike the barley dataset this was not largely a function of topography. The greater size variability observed in sorghum grains meant PC1 contained both a topographical and size contribution. PC3 and PC4 contained both physical and chemical variation that could not easily be separated. Variation explained by PC3 seemed to be due to proximate chemical composition, whereas the variation explained by PC4 could already have been due to the onset of germination with the release of enzymes.

3.3. Wheat

A distinct difference between viable and non-viable wheat kernels was not observed until PC6 [8]. The PC1–PC6 score images of viable and non-viable wheat kernels are shown in Fig. 7. Score values grouped around zero of PC1 (light blue and green) were associated with the flat dorsal side of the kernel. The edges of the wheat kernels had negative PC1 score values (red and dark blue in Fig. 7) and positive PC1 score values (yellow) were associated with the lower apex or small end as well as the germ end of the kernels. Principal component one loadings of the wheat dataset were similar to both the barley and sorghum datasets, confirming the explained variation being due to physical and thus scattering differences (Fig. 8).

The kernel edges (possible shading effect) had negative PC2 score values (red, dark blue and light blue in Fig. 7) and the higher dorsal side positive PC2 score values (green, yellow and orange). Overall the PC4 score image exhibited the same trend as PC2. The opposite was observed in PC3 with the higher dorsal side having negative score values. PC2 and PC3 loading line plots for the wheat image were similar to that of PC3 of the barley image dataset, while the loading line plot of PC4 for wheat was similar to that of PC2 of the barley image dataset. Within the scores image of PC5 a weak distinction between viable and non-viable kernels was observed, however, PC5 was largely characterised by negative scores (red) on the lower edges of the kernels. The loadings of PC5 clearly indicated this PC described chemical differences. In PC6 negative values (red and dark blue) were associated with viable kernels and positive values (light blue and green) with non-viable kernels. Again a reduction of baseline differences in the SNV corrected average spectra between each set of PC groups was observed with increasing PC.

Of the three grains the wheat score images were the most complex. For example, the first PC did not explain variation due to kernel shape as clearly as was observed in the barley and sorghum image datasets, respectively. This could be due to the dorsal side of wheat grain being more flat compared to the other two grains. It is suggested that this could also have been a function of the difference in seed coat (or hull) texture of wheat compared to that of barley and sorghum. A highly textured surface will result in variable scattering across the sampling area that cannot be explained within a single PC but rather influences several PCs.

4. Conclusions

Kernel topography clearly influences NIR-HSI spectral data collection and subsequent analysis and interpretation. Topography, in terms of kernel shape and surface roughness, was a source of variation isolated within PCs, despite spectral preprocessing with standard normal variate transformation. Both the chemical and the topographical complexity of the grains being investigated influenced the ability of PCA to separate the various sources of spectral variation. The complex topographies of grains required spectral preprocessing and more than a single PC to be explained efficiently. The first PC of each grain dataset was always due to effects attributed to the kernel surface, thus scattering; although less prominent for the wheat image. The subsequent PCs were

dominated by either physical effects or chemical information from within the kernel. For example, PC2 of the barley image dataset illustrated the difference between embryo and endosperm explaining the proximate composition of the kernel. This was independent of grain type studied; in each dataset similar loadings were observed, though the order was different in the case of wheat. A full understanding of a spectral image dataset using PCA is only possible when all PCs, before the PC of interest, are interpreted. The possible influence of penetration depth in association with scattering should also be considered in greater detail. Future studies will require larger populations to better define chemical and physical variation, and should explore other data analysis methods or preprocessing techniques to make the viability effects more prominent in higher variance PCs. In addition, adaptation of hardware should be investigated to reduce the combined effect of illumination and topography.

Acknowledgements

Samples were kindly provided by the Agricultural Research Council – Small Grain Institute, PANNAR and South African Breweries Malting. This project was funded by the Winter Cereal Trust (South Africa) and the Sorghum Trust (South Africa). Paulina Engelbrecht wishes to thank Stellenbosch University and FoodBev SETA for Masters bursaries. Cushla McGoverin acknowledges funding for postdoctoral research provided by the National Research Foundation, South Africa (Grant number 71390). In addition, the South African-Swedish Research Partnership Programme Bilateral Agreement, NRF, (UID 60958) is acknowledged for funding to work at the Swedish University of Agricultural Sciences (VR 348-2006-6715). We are also grateful to Oskar Jonsson (Umbio AB, Umea, Sweden) for the use of the SisuCHEMA imaging system, Evince software and assistance with imaging.

References

[1] W.F. McClure, in: Y. Ozaki, W.F. McClure, A.A. Christy (Eds.), Near-infrared Spectroscopy in Food Science and Technology, John Wiley & Sons, Inc., Hoboken, 2007, pp. 1–10.
[2] E.N. Lewis, L.H. Kidder, in: S. Sasic, Y. Ozaki (Eds.), Raman, Infrared and Near-infrared Chemical Imaging, John Wiley & Sons, Inc, Hoboken, 2010, pp. 75–92.
[3] J. Burger, P. Geladi, J. Near Infrared Spectrosc. 15 (2007) 29–37.
[4] J. Burger, P. Geladi, J. Chemometr. 19 (2005) 355–363.
[5] A.A. Gowen, C.P. O'Donnell, M. Taghizadeh, P.J. Cullen, J.M. Frias, G. Downey, J. Chemometr. 22 (2008) 259–267.
[6] E. Gaston, J.M. Frias, P.J. Cullen, C.P. O'Donnell, A.A. Gowen, J. Agric. Food Chem. 58 (2010) 6226–6233.
[7] M. Manley, G. du Toit, P. Geladi, Anal. Chim. Acta 686 (2010) 64–75.
[8] C.M. McGoverin, P. Engelbrecht, P. Geladi, M. Manley, Anal. Bioanal. Chem. 401 (2011) 2283–2289.
[9] P. Engelbrecht, Near infrared hyperspectral imaging as detection method for pre-germination in whole wheat, barley and sorghum grains. Masters Thesis, Stellenbosch University, Stellenbosch, 2011.
[10] P. Williams, M. Manley, G. Fox, P. Geladi, J. Near Infrared Spectrosc. 18 (2010) 49–58.
[11] K. Esbensen, P. Geladi, Chemometr. Intell. Lab. 7 (1989) 67–86.
[12] B.G. Osborne, T. Fearn, P.H. Hindle, Practical NIR Spectroscopy with Applications in Food and Beverage Analysis, Longman Scientific & Technical, Harlow, 1993.